

Journal of Biomedical Optics

BiomedicalOptics.SPIEDigitalLibrary.org

Monitoring of interaction of low-frequency electric field with biological tissues upon optical clearing with optical coherence tomography

Adrián F. Peña
Alexander Doronin
Valery V. Tuchin
Igor Meglinski

SPIE.

Monitoring of interaction of low-frequency electric field with biological tissues upon optical clearing with optical coherence tomography

Adrián F. Peña,^{a,b} Alexander Doronin,^a Valery V. Tuchin,^{c,d,e} and Igor Meglinski^{a,c,*}

^aUniversity of Otago, The Jack Dodd Centre for Quantum Technology, Department of Physics, P.O. Box 56, Dunedin, 9054 New Zealand

^bUniversidad Autónoma de Tamaulipas, Centro Universitario Tampico Madero, CP 89109, México

^cSaratov State University, Research-Educational Institute of Optics and Biophotonics, 83 Astrakhanskaya Street, Saratov, 410012 Russia

^dInstitute of Precise Mechanics and Control, Russian Academy of Science, Laboratory of Laser Diagnostics of Technical and Living Systems, 24 Rabochaya Street, Saratov, 410028 Russia

^eUniversity of Oulu, Optoelectronics and Measurement Techniques Laboratory, P.O. Box 4500, Oulu, FI-90014, Finland

Abstract. The influence of a low-frequency electric field applied to soft biological tissues *ex vivo* at normal conditions and upon the topical application of optical clearing agents has been studied by optical coherence tomography (OCT). The electro-kinetic response of tissues has been observed and quantitatively evaluated by the double correlation OCT approach, utilizing consistent application of an adaptive Wiener filtering and Fourier domain correlation algorithm. The results show that fluctuations, induced by the electric field within the biological tissues are exponentially increased in time. We demonstrate that in comparison to impedance measurements and the mapping of the temperature profile at the surface of the tissue samples, the double correlation OCT approach is much more sensitive to the changes associated with the tissues' electro-kinetic response. We also found that topical application of the optical clearing agent reduces the tissues' electro-kinetic response and is cooling the tissue, thus reducing the temperature induced by the electric current by a few degrees. We anticipate that dcOCT approach can find a new application in bioelectrical impedance analysis and monitoring of the electric properties of biological tissues, including the resistivity of high water content tissues and its variations. © 2014 Society of Photo-Optical Instrumentation Engineers (SPIE) [DOI: 10.1117/1.JBO.19.8.086002]

Keywords: optical coherence tomography; electric field; optical clearing; biological tissues; electro-kinetic response; temperature; bioelectrical impedance.

Paper 140355R received Jun. 4, 2014; revised manuscript received Jul. 13, 2014; accepted for publication Jul. 14, 2014; published online Aug. 6, 2014.

1 Introduction

Optical coherence tomography (OCT) is a well-known imaging diagnostic modality widely used for noninvasive imaging of soft biological tissues both *in vivo* and *in vitro* with high spatial resolution (3 to 5 μm) and up to a few millimeters probing depth.¹⁻⁴ After being significantly improved, OCT has generated major interest as a tool for clinical diagnostics.^{5,6} By using spatial and/or temporal analysis of the dynamic speckle patterns generated by moving red blood cells, various OCT modifications for visualization of subcutaneous blood vessels' distribution in human skin *in vivo* have been suggested, including speckle variance OCT (svOCT),⁷ optical microangiography (OMAG),⁸ correlation map OCT (cmOCT),⁹ and double correlation OCT (dcOCT).¹⁰ It has also been demonstrated that the dcOCT approach can be used for visualization of molecular diffusion within the skin tissues *in vivo*^{11,12} and for direct imaging of the electro-kinetic response of biological tissues *ex vivo*.¹³

In the current paper, we present the results of further OCT studies of the electro-kinetic response of biological tissues influenced by a low-frequency electric field at normal conditions and upon the topical application of optical clearing agents (OCAs). The tissues' optical clearing is widely described elsewhere¹⁴⁻¹⁸ and is based on refractive index matching between tissues'

structural compounds and OCA diffused into the tissues and tissue dehydration due to the osmotic properties of OCAs. Topical application of OCAs enhances light penetration depth and significantly increases the OCT image contrast.¹⁹⁻²³ Therefore, following the results of recent studies of the interaction of low-frequency electric fields with biological tissues by OCT,^{13,24} we apply a 50% glycerol solution in water as an OCA to enhance the image contrast and possibly observe the spatial distribution of the electric field within the tissues. Bearing in mind that hyperosmotic OCAs may induce dehydration and corresponding alteration of tissues' morphological and optical properties,¹⁷ in addition to OCT imaging, measurements of thermal profiles and impedance at normal conditions and upon optical clearing have been done.

2 Method and Materials

For the experimental setup (Fig. 1), a standard swept-source OCT (OCM1300SS, Thorlabs Inc., Newton) operated in a polarization-sensitive mode without phase retardation has been used to acquire both two-dimensional (2-D) and three-dimensional (3-D) images of *ex vivo* biological tissues. The OCT experimental system consists of the swept-source engine, imaging module, and imaging probe. The swept source has a central wavelength of 1325 nm with a bandwidth of

*Address all correspondence to: Igor Meglinski, E-mail: igor.meglinski@otago.ac.nz

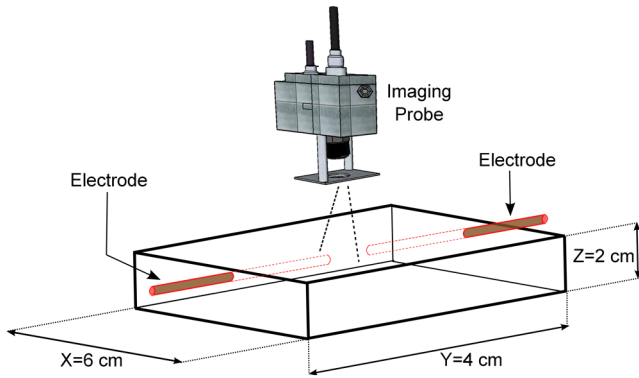


Fig. 1 Schematic presentation of the experiment. The standard optical coherence tomography (OCT) probe (OCM1300SS, Thorlabs Inc., Newton) is placed above the surface of tissue sample to acquire OCT images from the area between two electrodes embedded into the tissue at ~ 0.5 mm depth and separated by ~ 5 to 6 mm from each other.

~ 100 nm, a scanning rate of 16 kHz, and an output power of the probing light of 12 mW. The system is capable of acquiring a 3-D volume of $1024 \times 1024 \times 512$ pixels (i.e., up to $10 \text{ mm} \times 10 \text{ mm} \times 3 \text{ mm}$) containing 1024 images within ~ 40 s, with respective axial and lateral resolutions of ~ 13 and ~ 25 μm . A function generator (GFG 2100, ISO-TECH, Corby, England) has been used to apply an alternating current (ac) of fixed frequency and voltage to tissue by means of two stainless steel electrodes. The ends of the electrodes were separated from each other by ~ 1.5 cm, as presented in Fig. 1.

To quantify the effect of the influence of a low frequency-electric field in the tissue samples, we use the dcOCT approach developed earlier.¹⁰ Within the framework of the dcOCT approach, the similarity between images is accessed by sequential applications of the Wiener filter and by performing cross-correlation. The idea behind dcOCT is that a difference between the regions of low correlation corresponding to motion or tissues' alterations induced by the external electric field and the regions of high correlation correspond to static structures. To quantitatively assess the relative strength of the applied electric field in tissue, the mean of the cross-correlation values is evaluated.¹³

Figure 2 schematically shows this procedure with application to the obtained OCT images of the *ex vivo* tissue samples.

In the first step of the double correlation approach, by utilizing the adaptive Wiener filtering procedure, the background noise is suppressed and the OCT image artifacts (such as blur, physical offsets of tissue boundaries) are removed. Creation of the Wiener filter $I_w(x, z)$ requires calculation of the filter's coefficients by obtaining autocorrelation functions of the OCT signal $P_S[I(x, z)]$ and noise $P_N[I(x, z)]$. In the frequency domain, the Wiener filtering image is defined as^{25,26}

$$I_w(x, z) = \frac{P_S[I(x, z)]}{P_S[I(x, z)] + P_N[I(x, z)]}. \quad (1)$$

Here, $P_N[I(x, z)]$ is estimated by calculation of the local variance using 2-D correlation.²⁶ Following subtraction of an estimate of the noise from the original OCT images, the cross-correlation between two grids is calculated as^{10,13}

$$C(x, z) = \mathcal{F}^{-1}\{\mathcal{F}[I_w(t)] \times \overline{\mathcal{F}[I_w(t+1)]}\}, \quad (2)$$

where

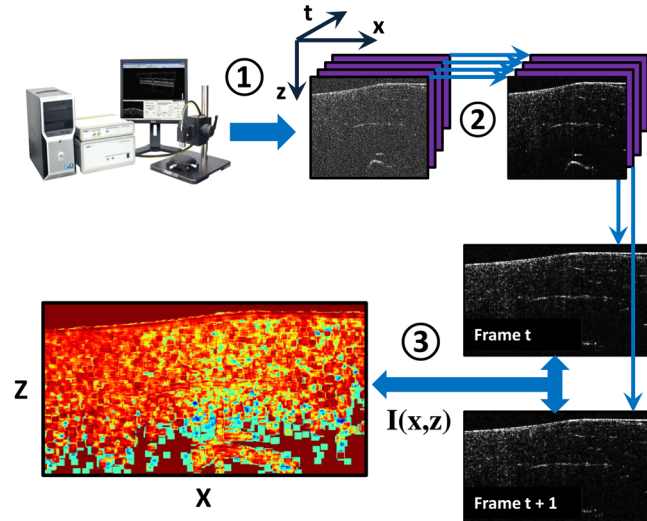


Fig. 2 Schematic presentation of double correlation OCT (dcOCT) approach. Step 1 corresponds to $I(x, z)$ image acquisition by conventional OCT. Step 2 shows the Wiener filtering of the obtained images. Step 3 represents the cross-correlation procedure between the Wiener filtering images $I_w(x, z)$ obtained at t and $t+1$ time intervals and the generation of correlation map defined by Eq. (2).

$$\mathcal{F}[I_w(t)] = \sum_{x=0}^{M-1} \sum_{z=0}^{N-1} I_w(x, z) e^{-2\pi i(ux/M + vz/N)}. \quad (3)$$

Here, $\mathcal{F}[I_w(t)]$ is the Fourier transform of $I_w(t)$ and $\overline{\mathcal{F}[I_w(t+1)]}$ is the complex conjugate of the Fourier transform $\mathcal{F}[I_w(t+1)]$ of $I_w(t+1)$; u and v are spatial frequencies in the x and z directions, respectively. M and N are the maximum number of pixels in the x and z directions, and t is the time interval for image acquisition.

It should be pointed out that in cross-correlation analysis, the size of the grid should be carefully selected since it is a trade-off between the processing time and the final quality of the outcome.⁹ If a grid is too big (e.g., 40×40 pixels), blurring and a loss of structural signal will occur.⁹ For a small grid (e.g., 5×5 pixels), the background noise will have a significant impact on the structural signal, resulting in decorrelation. In this study, a grid size of 7×7 was used to quantify the effect of influence of a low-frequency electric field in a fresh tissue sample.

Finally, the relative magnitude of influence of the low-frequency external electric field on the biological tissue is assessed as¹³

$$\Psi = 1 - \frac{1}{M \times N} \sum_{x=0}^{M-1} \sum_{z=0}^{N-1} C(x, z). \quad (4)$$

To speed up the computations, image analysis was performed on NVIDIA graphics processing units (GPUs) utilizing a compute unified device architecture parallel computing platform. The entire 3-D OCT volume of $1024 \times 1024 \times 512$ pixels containing 1024 images was processed on dual Tesla M2090 GPUs in ~ 30 s.¹⁰ The particular details of implementation are beyond the scope of this paper and are described elsewhere.¹⁰

Chicken breast pectoralis (6 to 7 weeks old), obtained from a primary supplier, were used in the experiments. A thermal camera (FLIR i3, FLIR Systems Inc., Wilsonville) was used to determine

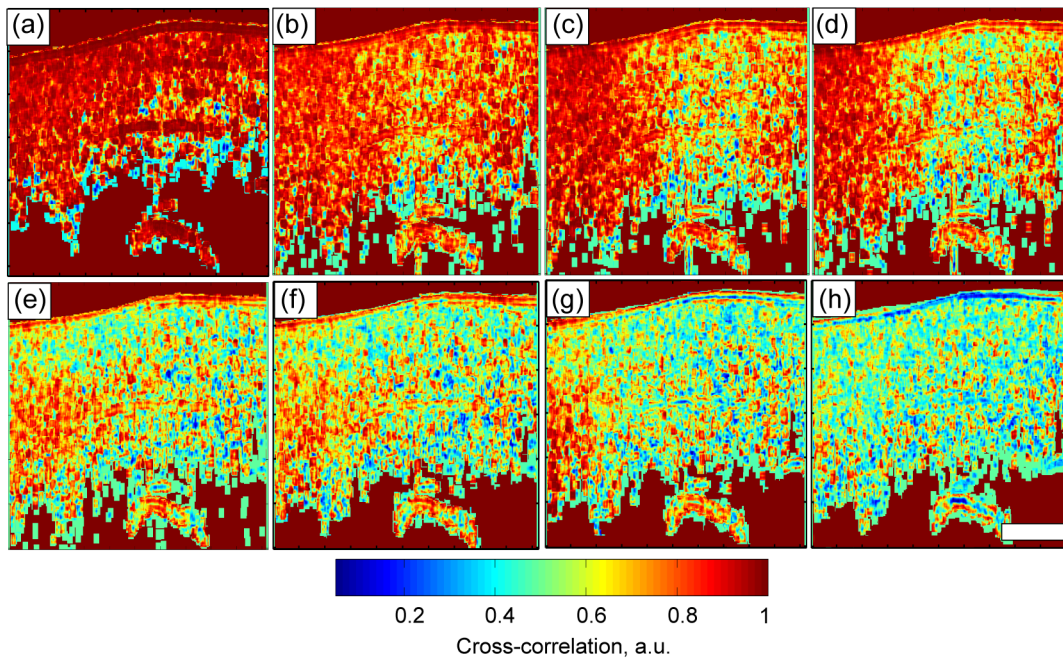


Fig. 3 Two-dimensional (2-D) dcOCT images $C(x, z)$ of fresh chicken breast (pectoralis) *ex vivo* obtained during exposure with 10 V and 1 Hz alternating current at 0, 1, 4, 60, 120, 200, 450, and 600 s after topical application of 50% water-glycerol solution: images from (a) to (h), respectively. Scale bar corresponds to 250 μm .

the rise in temperature of the tissue due to the exposure of an electric field. The camera provides a thermal image quality of 60×60 pixels with a field of view of $12.5 \text{ deg}(H) \times 12.5 \text{ deg}(V)$, and a thermal sensitivity of 0.15°C . During the experiment, the thermal camera and OCT probe were placed to acquire thermal profiles and OCT images from the area between the electrodes. The measurements of resistance between the electrodes

across the tissue sample were done by using a standard multi-meter (M2005, AVO International, Dover, England).

3 Results and Discussion

The results of the dcOCT imaging approach with and without topical application of OCA are presented in Figs. 3 and 4, respectively. In both figures, 2-D correlation images $C(x, z)$

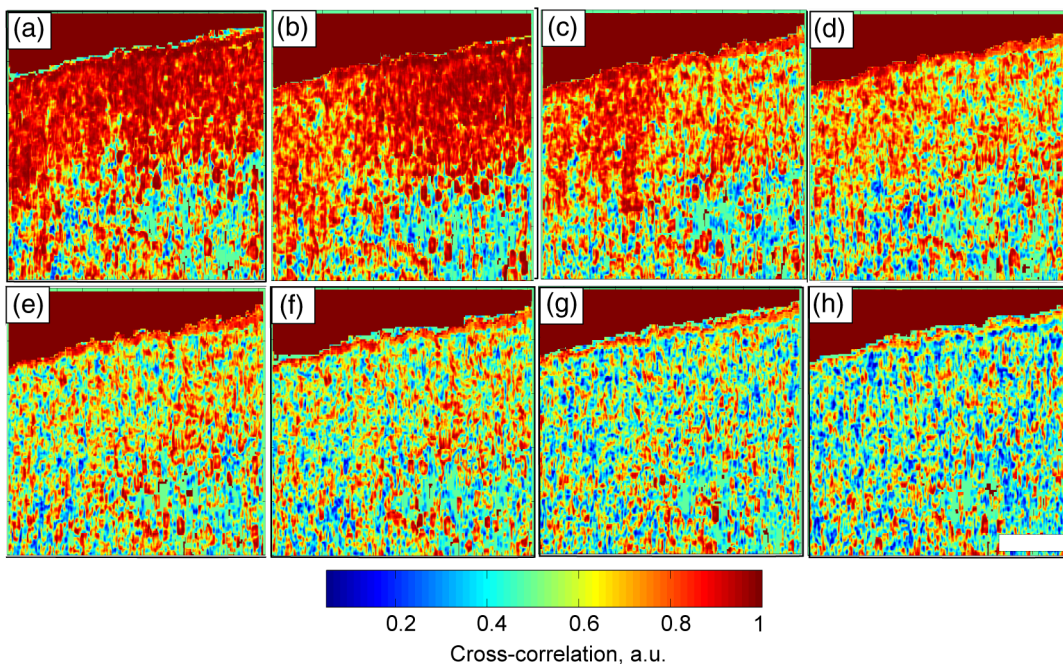


Fig. 4 2-D dcOCT images $C(x, z)$ of fresh chicken breast (pectoralis) *ex vivo* obtained during exposure with 10 V and 1 Hz alternating current at normal conditions at same time intervals as presented in Fig. 3. Scale bar corresponds to 250 μm .

are obtained at the same time intervals, i.e., 0, 1, 4, 60, 120, 200, 450, and 600 s.

Figure 5 shows the relative magnitude of the influence of the electric field on tissue as a function of time, obtained by Eq. (4) for the images presented in Figs. 3 and 4.

As one can see, the fluctuations induced by the electric field within the biological tissues are exponentially increased in time (see Fig. 5). The relative magnitude of influence of the electric field on biological tissue becomes lower when the tissue sample is exposed with the optical clearing that provides an observation of higher correlations between 2-D OCT images. It can be conceived that at low frequency, when an electrical field is applied, the charged ions move actively in the tissue sample exposed with the optical clearing agent rather than in a tissue sample under normal conditions.²⁷

Figures 6 and 7 show the evolution of thermal profiles measured at the surface of the chicken breast sample during the exposure of 10 V–1 Hz ac electric current without and with topical application of OCA. In both cases, the thermal IR camera was focused at the surface of the sample between the electrodes. Figures 6(a)–6(d) and 7(a)–7(d) present thermal profiles taken at 0, 5, 7.5, and 10 min, respectively.

As one can see, at normal conditions the temperature at the tissue surface reaches a maximum value of $\sim 26^{\circ}\text{C}$ in the area between the two electrodes (see Fig. 6), while the rise of temperature upon optical clearing is 1 deg less (see Fig. 7). It should also be pointed out that the kinetics of temperature changes is different for the samples with and without optical clearing exposure. Apparently, optical clearing slightly cools the biological tissues, thus reducing the temperature induced by the electric current by a few degrees.

The changes of temperature within the tissue sample induced by the electric current are likely attributed to variations in tissue resistance. Therefore, Fig. 8 shows the results of resistance measurements taken in parallel with temperature monitoring.

The resistance of the tissue sample measured at normal conditions is mostly constant and is reduced in ~ 7.5 min due to the temperature increase (see Fig. 8). When OCA is topically applied, the resistance of the high water-content tissue²⁸ slightly

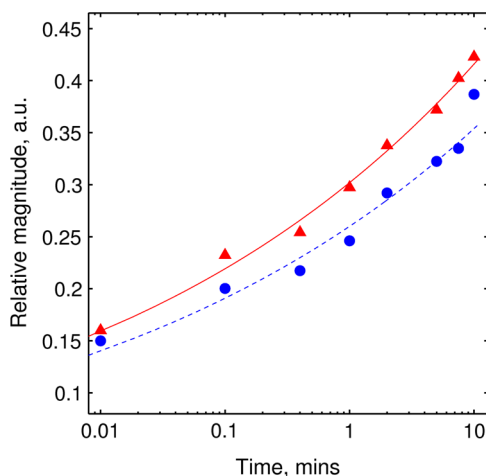


Fig. 5 Relative magnitude of influence of the electric field on tissue as a function of time: triangles represent the results for tissue sample without optical clearing and circles represent the results for tissue sample topically exposed by optical clearing agent (OCA). The solid and dashed lines show the results of best fitting for tissue sample without and with topical application of OCA, respectively.

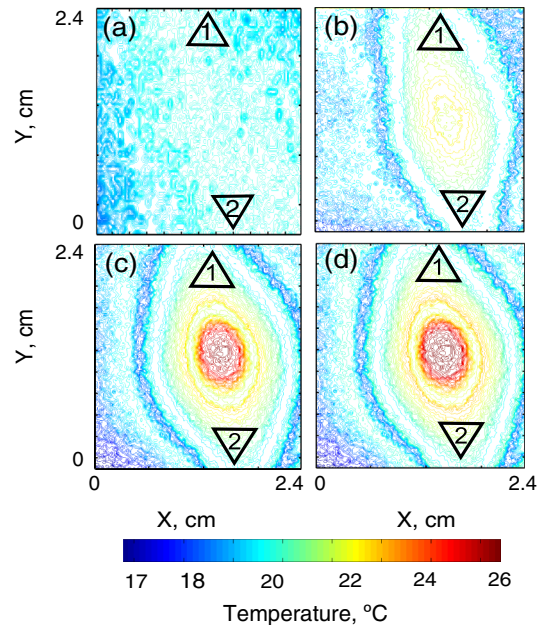


Fig. 6 Thermal profiles of fresh chicken breast (pectoralis) *ex vivo* exposed with 10 V and 1 Hz alternating current at normal conditions, i.e., without an optical clearing. (a), (b), (c), and (d) represent thermal profiles taken at 0, 5, 7.5, and 10 min, respectively. Triangles 1 and 2 show the electrode positions under the tissue surface.

increases (see Fig. 8). This is not necessarily in contradiction with the findings of this study. Topical application of OCA onto the surface of the tissue samples temporarily pushes water from the subsurface area out of the sampling volume, producing dehydration of topical tissue layers.^{14–18} Therefore, the resistance measured at the subsurface area, i.e., in the area of main localization of current flows, increases. Eventually, in ~ 7.5 min, due to rehydration of upper tissue layers from in-depth layers, a decrease in resistance is observed (see Fig. 8).

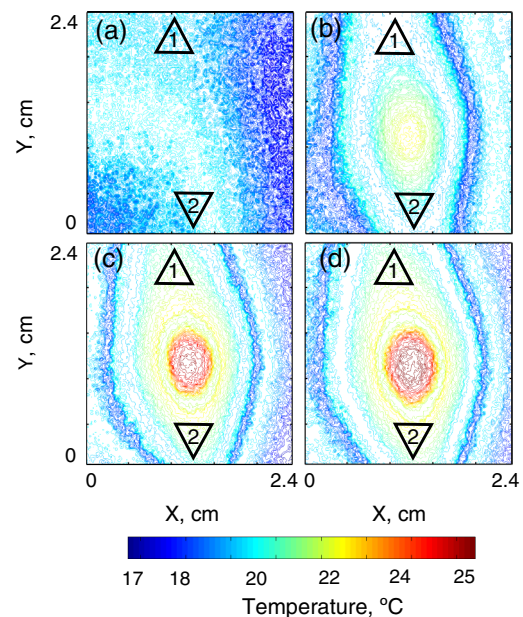


Fig. 7 Thermal profiles of tissue exposed with 10 V and 1 Hz alternating current taken after topical application of 50% glycerol solution in water at same time intervals as in Fig. 6.

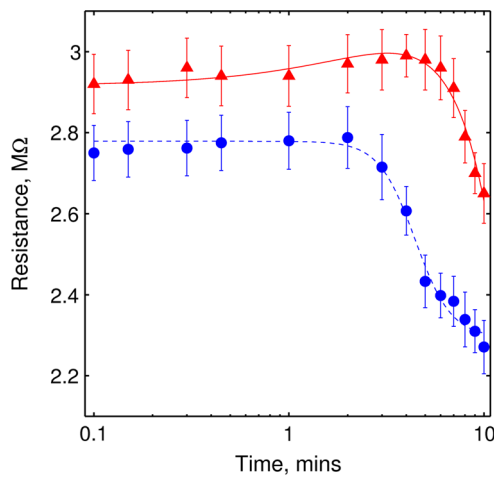


Fig. 8 Results of resistance measurements across the tissue sample as a function of time corresponding to the thermal profile measurements (see Figs. 6 and 7). Triangles and circles are, respectively, tissue with and without exposure of an OCA. The solid and dashed lines show the results of best fittings.

Many applications of bioelectrical impedance spectroscopy are based on the assumption of considerable differences between resistivity for high water-content tissues, but due to large confidence intervals, these differences are difficult to quantitatively observe.^{27,28} However, with the current dcOCT approach, the current flow as well as the temperature and resistance variations can be assessed with and without application of OCA.

4 Conclusions

The electro-kinetic response of tissues has been observed and quantitatively evaluated by the dcOCT approach, utilizing consistent application of an adaptive Wiener filtering and a Fourier domain correlation algorithm. The results show that fluctuations induced by the electric field within the biological tissues are exponentially increased in time. We demonstrate that in comparison to the measurements of the resistance and temperature profiles at the surface of the tissue samples, the dcOCT approach is an order higher in sensitivity to the changes associated with the tissues' electro-kinetic response. We also found that topical application of optical clearing reduces the tissues' electro-kinetic response and cools the tissue, thus reducing by a few degrees the temperature induced by the applied electric current. We anticipate that the dcOCT approach can find a new application similar to bioelectrical impedance spectroscopy for monitoring the electro-optical properties of biological tissues, such as human skin, and their variations resulting from a transdermal drug or health-care products diffusion.

Acknowledgments

The authors acknowledge useful discussion and constructive comments provided by Dr. Vyacheslav Kalchenko (Weizmann Institute of Science, Israel) during the paper preparation. A.F.P. thanks Consejo Nacional de Ciencia y Tecnología CONACYT, México, for the scholarship provided. V.V.T. is grateful for partial support by Russian Presidential grant NSh-703.2014.2, the Government of the Russian Federation (grant 14.Z50.31.0004) to support scientific research projects implemented under the supervision of leading scientists, and FiDiPro, TEKES

Program (40111/11), Finland. The authors also acknowledge the support provided by the Department of Physics, University of Otago, New Zealand.

References

1. B. Bouma and G. Tearney, *Handbook of Optical Coherence Tomography*, Marcel Dekker, New York (2002).
2. V. V. Tuchin, *Coherent-Domain Optical Methods: Biomedical Diagnostics, Environmental Monitoring, and Material Science*, Vol. 1, Springer-Verlag, Berlin, Heidelberg, N.Y. (2013).
3. M. Brezinski, *Optical Coherence Tomography and Applications*, 1st ed., Academic Press, Elsevier, Burlington, MA (2006).
4. W. Drexler and J. Fujimoto, *Optical Coherence Tomography, Technology and Its Applications*, Springer, Berlin Heidelberg (2008).
5. A. M. Zysk et al., "Optical coherence tomography: a review of clinical development from bench to bedside," *J. Biomed. Opt.* **12**(5), 051403 (2007).
6. R. Hamdan et al., "Optical coherence tomography: from physical principles to clinical applications," *Arch. Cardiovasc. Dis.* **105**(10), 529–534 (2012).
7. A. Mariampillai et al., "Speckle variance detection of microvasculature using swept-source optical coherence tomography," *Opt. Lett.* **33**(13), 1530–1532 (2008).
8. R. K. Wang et al., "Depth-resolved imaging of capillary networks in retina and choroid using ultrahigh sensitive optical microangiography," *Opt. Lett.* **35**(9), 1467–1469 (2010).
9. E. Jonathan, J. Enfield, and M. J. Leahy, "Correlation mapping method for generating microcirculation morphology from optical coherence tomography (OCT) intensity images," *J. Biophotonics* **4**(9), 583–587 (2011).
10. A. Doronin and I. Meglinski, "Imaging of subcutaneous microcirculation vascular network by double correlation optical coherence tomography," *Laser Photon. Rev.* **7**(5), 797–800 (2013).
11. T. Rattanapak et al., "Transcutaneous immunization using micro-needles and cubosomes: mechanistic investigation using optical coherence tomography and two-photon microscopy," *J. Control. Release* **172**(3), 894–903 (2013).
12. T. Kamali et al., "Assessment of transcutaneous vaccine delivery by optical coherence tomography," *Laser Phys. Lett.* **9**(8), 607–610 (2012).
13. A. F. Peña et al., "Imaging of the interaction of low-frequency electric fields with biological tissues by optical coherence tomography," *Opt. Lett.* **38**(14), 2629–2631 (2013).
14. V. V. Tuchin et al., "Light propagation in tissues with controlled optical properties," *J. Biomed. Opt.* **2**(4), 401–417 (1997).
15. G. Vargas et al., "Use of an agent to reduce scattering in skin," *Lasers Surg. Med.* **24**(2), 133–141 (1999).
16. V. V. Tuchin, "Optical clearing of tissues and blood using the immersion method," *J. Phys. D: Appl. Phys.* **38**(15), 2497–2518 (2005).
17. V. V. Tuchin, *Optical Clearing of Tissues and Blood*, SPIE Press, Bellingham, Washington (2006).
18. D. Zhu et al., "Recent progress in tissue optical clearing," *Laser Photon. Rev.* **7**(5), 732–757 (2013).
19. S. G. Proskurin and I. V. Meglinski, "Optical coherence tomography imaging depth enhancement by superficial skin optical clearing," *Laser Phys. Lett.* **4**(11), 824–826 (2007).
20. R. K. Wang and V. V. Tuchin, "Optical tissue clearing to enhance imaging performance for OCT," in *Optical Coherence Tomography, Technology and Applications*, 1st ed., W. Drexler and J. G. Fujimoto, Eds., pp. 855–866, Springer, Berlin Heidelberg (2008).
21. M. Bonesi, S. G. Proskurin, and I. V. Meglinski, "Imaging of subcutaneous blood vessels and flow velocity profiles by optical coherence tomography," *Laser Phys.* **20**(4), 891–899 (2010).
22. C. Drew, T. E. Milner, and C. G. Rylander, "Mechanical tissue optical clearing devices: evaluation of enhanced light penetration in skin using optical coherence tomography," *J. Biomed. Opt.* **14**(6), 064019 (2009).
23. K. V. Larin et al., "Optical clearing for OCT image enhancement and in-depth monitoring of molecular diffusion," *IEEE J. Sel. Topics Quantum Electron.* **18**(3), 1244–1259 (2012).
24. K. Wawrzyn et al., "Imaging the electro-kinetic response of biological tissues with optical coherence tomography," *Opt. Lett.* **38**(14), 2572–2574 (2013).

25. R. Gonzalez and R. Woods, *Digital Image Processing*, 3rd ed., Prentice Hall, NJ (2008).
26. J. Lim, *Two-Dimensional Signal and Image Processing*, Prentice Hall, NJ (1989).
27. J.-P. Morucci et al., "Bioelectrical impedance techniques in medicine," *Crit. Rev. Biomed. Eng.* **24**(4–6), 223–678 (1996).
28. T. J. Faes et al., "The electric resistivity of human tissues (100 Hz–10 MHz): a meta-analysis of review studies," *Physiol. Meas.* **20**(4), R1–10 (1999).

Adrián F. Peña is a postdoctoral research fellow in the Biophotonics and Biomedical Imaging Research Group at the University of Otago, New Zealand. His current research interests include laser tissue interaction, noninvasive imaging techniques, optical coherence tomography (OCT), polarization sensitive OCT, photo-acoustic tomography, and applications of these optical diagnostic modalities in biology and medicine.

Alexander Doronin is a postdoctoral fellow working in the Biophotonics and Biomedical Imaging Research Group at the University of Otago, New Zealand. His research interests include light-tissue

interaction, Monte Carlo computational modelling, parallel programming on graphics processing units using NVIDIA compute unified device architecture, and optical imaging modalities such as OCT, polarization-sensitive OCT, Doppler OCT, photo-acoustic tomography and other.

Valery V. Tuchin is a professor and chairman of Optics and Biophotonics at Saratov State University. He is also the head of laboratory, Institute of Precision Mechanics and Control, RAS. His research interests include biophotonics, tissue optics, laser medicine, tissue optical clearing, and nano-biophotonics. He is a member of SPIE, OSA, and IEEE. He is a fellow of SPIE and has been awarded Honoured Science Worker of the Russia, SPIE Educator Award, and FiDiPro (Finland).

Igor Meglinski is the head of biophotonics and biomedical imaging at the Department of Physics of the University of Otago, New Zealand. His research interests lie at the interface between physics, medicine, and biological sciences, focusing on the development of new noninvasive imaging/diagnostic techniques and their application in medicine and biology. He is a member of OSA, senior member of IEEE, fellow of the Institute of Physics (London, UK), and fellow of SPIE.